J|A|C|S ARTICLES

Published on Web 10/06/2009

Left- and Right-Handed Alpha-Helical Turns in Homo- and Hetero-Chiral Helical Scaffolds

Nicholas E. Shepherd, Huy N. Hoang, Giovanni Abbenante, and David P. Fairlie*

Division of Chemistry and Structural Biology, Institute for Molecular Bioscience, University of Queensland, Brisbane, Qld 4072, Australia.

Received August 3, 2009; E-mail: d.fairlie@imb.uq.edu.au

Abstract: Proteins typically consist of right-handed alpha helices, whereas left-handed alpha helices are rare in nature. Peptides of 20 amino acids or less corresponding to protein helices do not form thermodynamically stable alpha helices in water away from protein environments. The smallest known water-stable right- (α_R) and left- (α_L) handed alpha helices are reported, each stabilized in cyclic pentapeptide units containing all L- or all D-amino acids. Homochiral decapeptides comprising two identical cyclic pentapeptides ($\alpha_R\alpha_R$ or $\alpha_L\alpha_L$) are continuous alpha-helical structures that are extremely stable to denaturants, degradative proteases, serum, and additives like TFE, acid, and base. Heterochiral decapeptides comprising two different cyclic pentapeptides ($\alpha_L\alpha_R$ or $\alpha_R\alpha_L$) maintain the respective helical handedness of each monocyclic helical turn component but adopt extended or bent helical structures depending on the solvent environment. Adding TFE to their aqueous solutions caused a change to bent helical structures with slightly distorted N-terminal α_R or α_L-helical turns terminated by a Schellman-like motif adjacent to the C-terminal α_L or α_R-turn. This hinge-like switching between structures in response to an external cue suggests possible uses in larger structures to generate smart materials. The library of left- and right-handed 1−3 turn alpha-helical compounds reported herein project their amino acid side chains into very different regions of 3D space, constituting a unique and potentially valuable class of novel scaffolds.

Introduction

There is great interest in designing and constructing small molecules that can reproduce complex polypeptide shapes in chemically stable structures for potential applications to materials and biological research or as new diagnostics or therapeutics.[1] Approaches used to control peptide structural elements, such as helices, strands and sheets, turns and loops, include exploiting weak interactions (hydrogen bonding, electrostatic, and hydrophobic),[2] addition of molecular templates that initiate or stabilize particular types of structure,[3] or insertion of unnatural constraints, which dictate backbone torsional angles and/or restrict conformational freedom (e.g., α,α-disubstituted, β- and γ-amino acids, macrocyclization).[3f,4]

A less common but important structure in nature is the left-handed α-helix (α_L), which is composed of D-amino acids.[5] Compared to the right-handed α-helix (α_R), both the occurrence (0.4% vs 30%) and length (3−4 residues) of α_L is much smaller in nature.[6] However, D-residues can confer important properties to peptides and proteins such as resistance to proteolytic cleavage and metabolism. Synthetic all D-residue analogues (inversomers) of naturally occurring α-helices have for example generated α_L-helical inhibitors of HIV fusion[7] and amyloid formation.[8] Left-handed α-helical structures composed of D-residues are capable of forming bundles with themselves and with right-handed α-helices.[8] There are examples of synthetic molecules composed of left- and right-handed helical segments

(1) *Acc. Chem. Res.* **2008**, *41*, 10, 1231−1438, full issue.
(2) Hughes, R. M.; Waters, M. L. *Curr. Opin. Struct. Biol.* **2006**, *16*, 514–524.
(3) (a) Kemp, D. S.; Curran, T. P.; Davis, W. M.; Boyd, J. G.; Muendel, C. *J. Org. Chem.* **1991**, *56*, 6672–6682. (b) Kemp, D. S.; Curran, T. P.; Boyd, J. G.; Allen, T. J. *J. Org. Chem.* **1991**, *56*, 6683–6697. (c) Gani, D.; Lewis, A.; Rutherford, T.; Wilkie, J.; Stirling, I.; Jenn, T.; Ryan, M. D. *Tetrahedron* **1998**, *54*, 15793–15819. (d) Lewis, A.; Ryan, M. D.; Gani, D. *J. Chem. Soc., Perkin Trans. 1* **1998**, 3767–3775. (e) Lewis, A.; Wilkie, J.; Rutherford, T. J.; Gani, D. *J. Chem. Soc., Perkin Trans. 1*. **1998**, 3777–3793. (f) Fairlie, D. P.; Abbenante, G.; March, D. R. *Curr. Med. Chem.* **1995**, *2*, 654–686. (g) Mueller, K.; Obrecht, D.; Knierzinger, A.; Stankovic, C.; Spiegler, C.; Bannwarth, W.; Trzeciak, A.; Englert, G.; Labhardt, A. M.; Schoenholzer, P. *Perspectives in Medicinal Chemistry* **1993**, 513–531. (h) Austin, R. E.; Maplestone, R. A.; Sefler, A. M.; Liu, K.; Hruzewicz, W. N.; Liu, C. W.; Cho, H. S.; Wemmer, D. E.; Bartlett, P. A. *J. Am. Chem. Soc.* **1997**, *119*, 6461–6472. (i) Kahn, M.; Kim, H.-O.; Urban, J. Molecumetics Ltd.: US5859184, 1999. (j) Hanessian, S.; Papeo, G.; Fettis, K.; Therrien, E.; Viet, M. T. P. *J. Org. Chem.* **2004**, *69*, 4891–4899. (k) Robinson, J. A. *Synlett* **2000**, *4*, 429–441. (l) Felix, F.; Gellman, S. H. *J. Am. Chem. Soc.* **2009**, *131*, 7970–7972.
(4) (a) Stigers, K. D.; Soth, M. J.; Nowick, J. S. *Curr. Opin. Chem Biol.* **1999**, *3*, 714–723. (b) Fairlie, D. P.; West, M. L.; Wong, A. K. *Curr. Med. Chem.* **1998**, *5*, 29–62. (c) Tanaka, M. *Chem. Pharm. Bull.* **2007**, *55*, 349–358. (d) Seebach, D.; Hook, D. F.; Glattli, A. *Biopolymers* **2006**, *84*, 23–37. (e) Martinek, T. A.; Mandity, I. M.; Fulop, L.; Toth, G. K.; Vass, E.; Miklos Hollosi, M.; Forro, E.; Fulop, F. *J. Am. Chem. Soc.* **2006**, *128*, 13539–13544.
(5) (a) Hung, L. W.; Kohmura, M.; Ariyoshi, Y.; Kim, S. H. *Acta Crystallogr., Sect., D: Biol. Crystallogr.* **1998**, *54*, 494–500. (b) Zawadzke, L. E.; Berg, J. M. *Proteins: Struct., Funct., Genet.* **1993**, *16*, 301–305. (c) Milton, R. C. D.; Milton, S. C. F.; Kent, S. B. H. *Science* **1992**, *256*, 1445–1448.
(6) Novotny, M.; Kleywegt, G. J. *J. Mol. Biol.* **2005**, *347*, 231–241.
(7) (a) Eckert, D. M.; Malashkevich, V. N.; Hong, L. H.; Carr, P. A.; Kim, P. S. *Cell* **1999**, *99*, 103–115. (b) Fisher, P. J.; Predergast, F. G.; Ehrhardt, M. R.; Urbauer, J. L.; Wand, A. J.; Sedarous, S. S.; McCormick, D. J.; Buckley, P. J. *Nature* **1994**, *368*, 651–653.
(8) Sia, S. K.; Kim, P. S. *Biochemistry* **2001**, *40*, 8981–8989.

capable of forming alternate conformations in organic solvents.[9] A computational study[10] recently provided interesting predictions about how left- and right-handed alpha helices in 11-residue peptides might interact in nature; however, experimentally these peptides are too short to adopt any defined structure in water and so predictions were not possible to test.

Here, we expand the available repertoire of secondary structural building blocks. We describe some cyclic pentapeptides, made up of five L- or five D-amino acids, which are the smallest water-stable right- and left-handed alpha-helical structures known, and we derive homo- and heterochiral decapeptide helices from various combinations of these structural building blocks. Solution structures, investigated for these helices by a combination of circular dichroism and 2D NMR spectroscopy, show unexpected differences in conformational behavior in response to an external cue. The library of minimalist alpha-helical structures created (α_L, α_R, $\alpha_R\alpha_R$, $\alpha_L\alpha_L$, $\alpha_L\alpha_R$, $\alpha_R\alpha_L$, $\alpha_L\text{Gly}\alpha_R$, $\alpha_R\text{Gly}\alpha_R$) represents a novel class of compounds with prospective uses as tools in chemical biology and as scaffolds for materials, chemical, and biological research.

Results and Discussion

Left- and Right-Handed Homochiral α-Helical Pentapeptides. We have previously reported the circular dichroism spectrum of Ac−R[KARAD]−NH_2, composed of six naturally occurring L-amino acids.[11] Here, we describe cyclic pentapeptide **1**, Ac-[KARAD]−NH_2, shown by CD spectra to be a right-handed α-helical structure, α_R (part A of Figure 1), and the smallest reported α helix corresponding to a single alpha-helical turn. Compound **2**, Ac−[karad]−NH_2, has been prepared from the five corresponding D-amino acids and it has the expected enantiomeric left-handed α-helical structure, as evidenced by the CD spectrum of identical molar elipticity wavelengths but intensities of *opposite* sign (part A of Figure 1). It is important to note two things in the context of what follows. First, the acyclic pentapeptide analogues of these compounds show no helical structure at all under these conditions (not shown). Second, the CD spectrum of a 1:1 mixture of **1** and **2** gave the expected null signal due to complete cancellation of their circular dichroism spectra (part A of Figure 1). There is also a slight shift in the expected minima/maxima (222→215 nm, 208→207 nm) for both right- and left-handed cyclic pentapeptides **1** and **2** compared with longer (>25 residue) polypeptide helices.[11] The thermal stability of monocycles **1** and **2** was briefly examined by monitoring the change in molar ellipticity at 215 nm with increasing temperature (part B of Figure 1). Both compounds underwent changes that led to a gradual decrease/increase in ellipiticty of exactly the same magnitude, indicating that they have exactly the same thermodynamic stability and do not completely unwind even at 85 °C.

1 and **2** gave identical 1D and 2D ^{1}H NMR spectral properties (Supporting Information), but the ROESY spectrum was too overlapped in the Hα region to deduce structures. Therefore, the structures were determined and compared for the hexapeptide analogues, Ac−R[KAAAD]−NH_2 (**3**) and Ac−r[kaaad]−NH_2 (**4**), with an arginine residue appended to the cyclic pentapeptide, this change producing well-dispersed 2D ^{1}H NMR spectra and

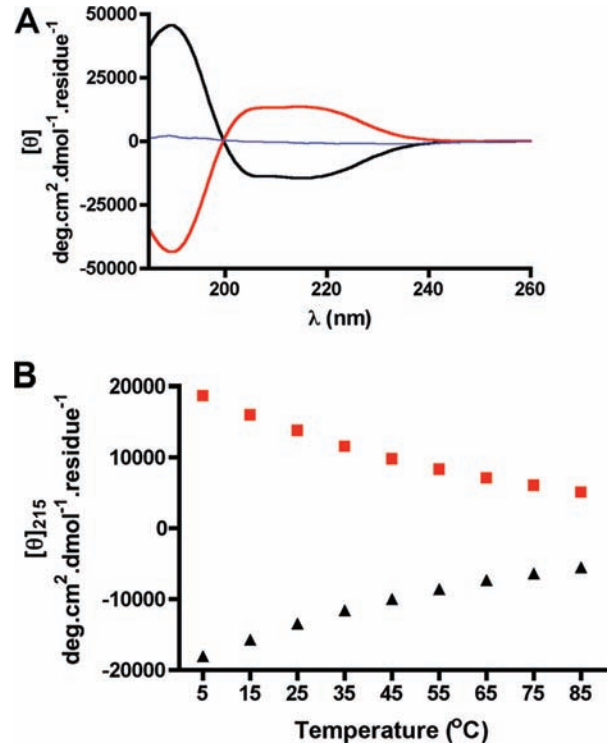

Figure 1. **A**: CD spectra for (**1**) Ac-[KARAD]−NH_2 (red, 250 μM), (**2**) Ac−[karad]−NH_2 (blue, 250 μM) and a 1:1 mixture of **1** and **2** (black, 125 μM each) in 10 mM phosphate buffer (pH 7.2, 298K) and **B**: Temperature dependence of molar ellipticity at 215 nm for 1 (▲) and 2 (red ■) over 5−85 °C.

over 50 distance restraints and 3 hydrogen-bond restraints for each structure. The structures clearly demonstrate that molecules **3** and **4** are indeed short right-handed (**3**) and left-handed (**4**) α-helices, mirror images of one another (Figure 2).

Left- and Right-Handed Homochiral α-Helical Decapeptides. Combinations of two homochiral pentapeptide macrocycles containing either all L- or all D-amino acids, Ac−[KARAD][KARAD]−NH_2 (**5**) and Ac−[karad][karad]−NH_2 (**6**), form stable right- and left-handed alpha-helical structures, each with 3 helical turns of 3.6 amino acids per turn, as evidenced by their CD spectra and NMR solution structures in water (Figure 3). A 1:1 mixture of **5** and **6** produces the expected null CD spectrum in aqueous solution (Figure 3), as expected for cancellation of the circular dichroism.

These homochiral $\alpha_R\alpha_R$ or $\alpha_L\alpha_L$ motifs are continuous alpha-helical structures that are extremely stable in water. Using CD spectral changes to monitor α-helix stability under different conditions, it was clear that adding denaturants (e.g., 8 M guandine), degradative proteases (e.g., trypsin), an acid, or a base did not affect α-helical content (Table 1). This technique is particularly sensitive for probing effects of such agents on peptide integrity and structure. By virtue of disrupting hydrogen bonding, the denaturant 8 M guanidine will unfold virtually all native protein and peptide structures, even those containing D-amino acids, so the preservation of the helix under those conditions is extraordinary. There were also no changes to the CD spectra when up to 50% TFE was present, and the compounds were also completely stable in normal human serum for at least 24 h (data not shown). This augurs well for the application of such helical scaffolds in different biological systems.

(9) (a) Banjeree, A. M.; Raghothama, S. R.; Karle, I.; Balaram, P. *Biopolymers* **1996**, *39*, 279–285. (b) Ousaka, N.; Inai, Y. *J. Am. Chem. Soc.* **2006**, *128*, 14736–14737.
(10) Nanda, V.; DeGrado, E. F. *J. Am. Chem. Soc.* **2006**, *128*, 809–816.
(11) Shepherd, N. E.; Hoang, H. N.; Abbenante, G.; Fairlie, D. P. *J. Am. Chem. Soc.* **2005**, *127*, 2974–2983.

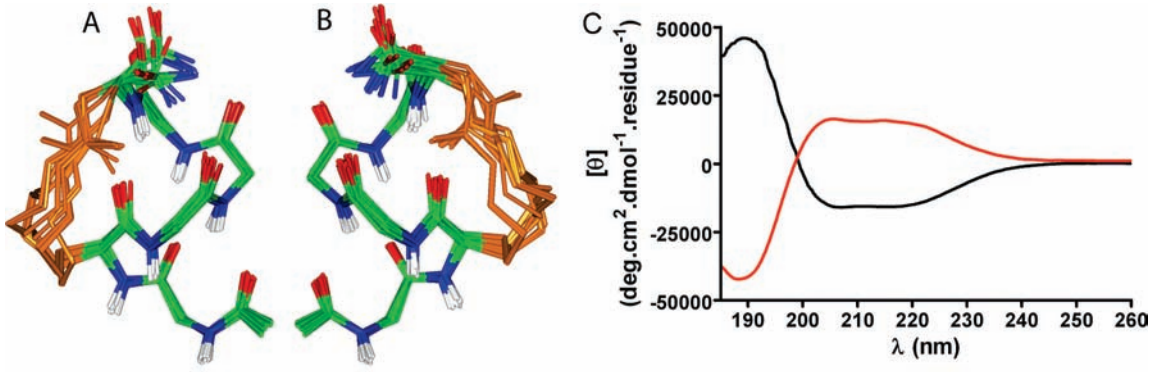

Figure 2. Solution structures derived by ROESY spectra for (**A**): Ac−R[KAAAD]−NH_2 (**3**) and (**B**): Ac−r[kaaad]−NH_2 (**4**) in 9:1 H_2O/D_2O, showing single right- and left-handed alpha-helical turns, respectively. Lys and Asp side chains with lactam linkage are in orange; N-terminus at bottom. (C) **3** (black) and **4** (red) at 150 μM concentrations in 10 mM PBS (pH 7.4) at 298 K.

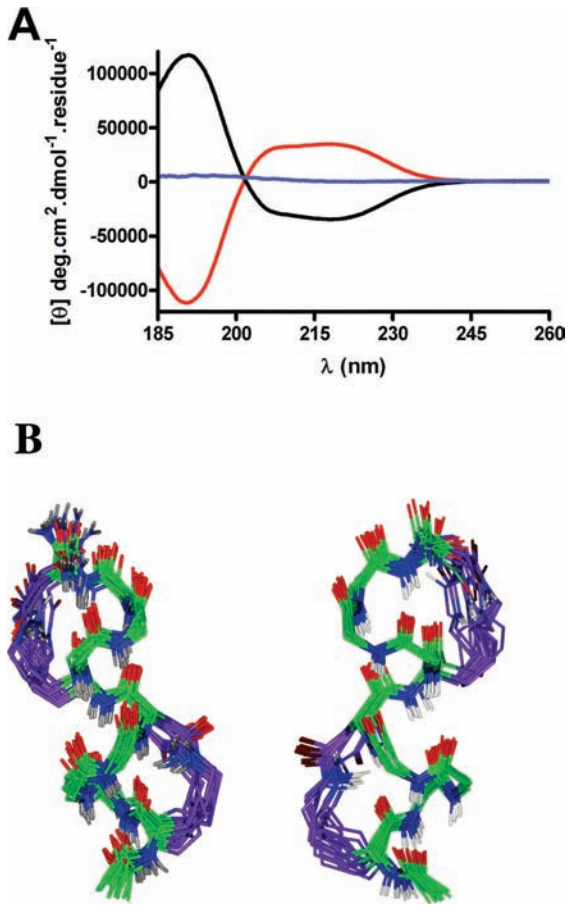

Figure 3. Structures for homochiral dimers, Ac−[KARAD]-[KARAD]−NH_2 (**5**) and Ac−[karad][karad]−NH_2 (**6**) with the N-terminus at the bottom. (**A**) CD spectra of **5** (black, 250 μM) and **6** (red, 250 μM) in 10 mM phosphate buffer (pH 7.2, 298 K) showing right- and left-handed alpha helicity, respectively. A 1:1 mix of **5** and **6** gave the expected null spectrum (blue). (**B**) Final 20 lowest energy NMR structures for **5** (left) and **6** (right) in H_2O/D_2O (9:1) at 288 K. All amide chemical shifts in **5** correspond to those in **6** and have the same temperature coefficients, NOEs in NOESY experiments, and produce mirror-image 3D structures.

Left- and Right-Handed Heterochiral α-Helical Decapeptides. With the aim of generating interesting new polypeptide scaffolds with defined shape, the all-L-residue pentapeptide macrocycle **1** was joined with the all-D-residue macrocycle **2** to generate heteochiral bicyclic decapeptides, Ac−[KARAD]-[karad]−NH_2 (**7**) and Ac−[karad][KARAD]−NH_2 (**8**). These bicyclic compounds gave identical 1D ^{1}H NMR spectra (Supporting Information) consistent with their enantiomeric relationship, and their CD spectra were recorded. If the respective monocyclic components of **7** and **8** maintained their structure and opposite handedness then both **7** and **8** would be expected to separately display a null CD spectrum. Part A of Figure 4 shows that **7** and **8** each give almost null linear CD spectra in aqueous buffer, with just a slight absorption in the 190 nm region. This almost complete cancellation of the optical signals from component cycles is consistent with each monocyclic component maintaining its respective helical structure and handedness within the decapeptide. Interestingly however, when 50% TFE was added to either **7** or **8**, the CD spectrum changed significantly (part B of Figure 4). For **7**, a large negative absorption at 190 nm and positive absorptions in the 205−220 nm region were observed, whereas for **8** a large positive absorption was observed at 190 nm and negative absorptions were observed in the 205−220 nm region. Overall, these spectra appeared to become α_R- and α_L-helical with the sign of the CD spectrum being dictated by the chirality of the C-terminal macrocyclic pentapeptide component. The results seemed to indicate that helicity was being lost in the N-terminal macrocycle but maintained in the C-terminal macrocycle.

Table 1. CD Molar Elipticity [Θ] (deg.cm^2.dmol^{-1}.residue^{-1}) for **6** in Different Aqueous Solutions and Conditions at 25C[a]

Solvent	$[\Theta]_{208}$	$[\Theta]_{222}$	$[\Theta]_{222}/[\Theta]_{222}$ in PBS
10 mM PBS (pH 7.2)	24 424	23 856	1.00
85 C	15 359	13 500	0.57
0.1 M acetic acid	24 020	24 040	1.01
0.1 M KOH	ND[b]	22 233	0.93
8 M guanidine	ND[b]	23 821	1.00
5 mg/L trypsin	20 007	20 209	0.85

[a] Reduction in helical content is reflected in changes in molar elipticity reletaive to 10 mM PBS (pH 7.2). [b] Not detectable at this wavelength.

Comparison of 1D NMR Data for 7 in Water versus TFE. To understand the effect of solvent on the CD spectra for Ac−[KARAD][karad]−NH_2 (**7**) in water versus TFE/water, ^{1}H NMR spectroscopy was used to examine **7** in H_2O/D_2O (9:1) and separately in H_2O/d_3-TFE (1:1). The changes in $^3J_{H\alpha\text{-}NH}$ were examined first (part A of Figure 5) as these give information about the backbone dihedral angles. In H_2O/D_2O (9:1), coupling constants below 6 Hz were observed for the first four residues of both the N-terminal L-macrocycle (Lys1, Ala2, Arg3, and Ala4) and C-terminal D-macrocycle (D-Lys6, D-Ala7, D-Arg8, D-Ala9) indicative of helical conformations. By contrast, in H_2O/d_3-TFE (1:1) coupling constants for the first four residues of

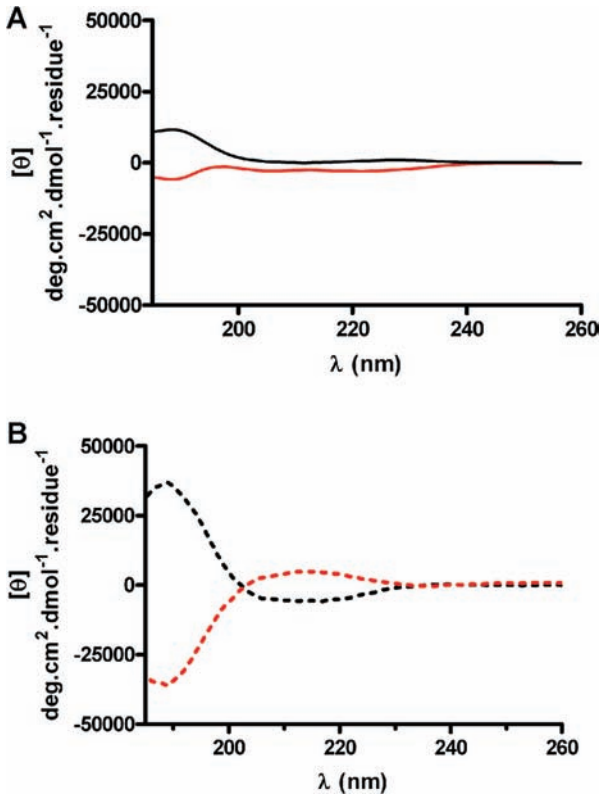

Figure 4. CD spectra for heterochiral bicyclic compounds Ac−[KARAD][karad]−NH_2 (**7**, 100 μM, red) and Ac−[karad]-[KARAD]−NH_2 (**8**, 100 μM, black) in 10 mM phosphate buffer (pH 7.2, 298 K) alone (**A**) or 1:1 TFE:phosphate buffer (**B**).

the C-terminal D-macrocycle remained below 6 Hz, however in the N-terminal L-macrocycle the coupling constant for Arg3 increased (5.61 to 6.66) indicating a change in dihedral angle from an α-helical value (−65 ± 30°) to a random coil value. The coupling constant of Asp5 also increased significantly (7.16−8.95 Hz), indicating a change in dihedral angle from a random coil value to a β-strand value (−120 ± 30°).

Changes in Hα chemical shift were also examined (Figure 5B). In H_2O/D_2O (9:1) Lys1-Ala4 and D-Lys6-D-Asp10 gave upfield shifts indicative of helical structures. In H_2O/d_3-TFE (1:1), Ala2-Ala4 and D-Lys6-D-Lys9 still displayed upfield shifts >0.1 ppm, however the magnitude of these shifts was much less compared to their respective upfield shifts in water. A significant downfield shift was observed in Asp5, indicating a change from a nonhelical to β-strand structure and in D-Asp10, which changed from a helical to random-type structure.

Finally, the temperature coefficients for amide protons between 278−313 K were examined (part C of Figure 5). In H_2O/D_2O (9:1) the amide protons of Ala4, D-Lys7, D-Arg8, D-Ala9, and one C-terminal amide proton (HT1) were less than 4 ppb/K, suggesting the involvement of these amide protons in hydrogen bonds. In H_2O/d_3-TFE (1:1), these same residues except for D-Arg8 appeared to be involved in hydrogen bonding along with new hydrogen bonds involving the amide proton of Arg3 and the amide proton in the N-terminal macrocyclic lactam bridge (HZ1).

Together this information suggests that a structural change is occurring particularly in the N-terminal L-macrocycle. There exists, however, the possibility that we are simply observing averaged values as two conformers interconvert. If averaged values were being observed then it seems reasonable to expect

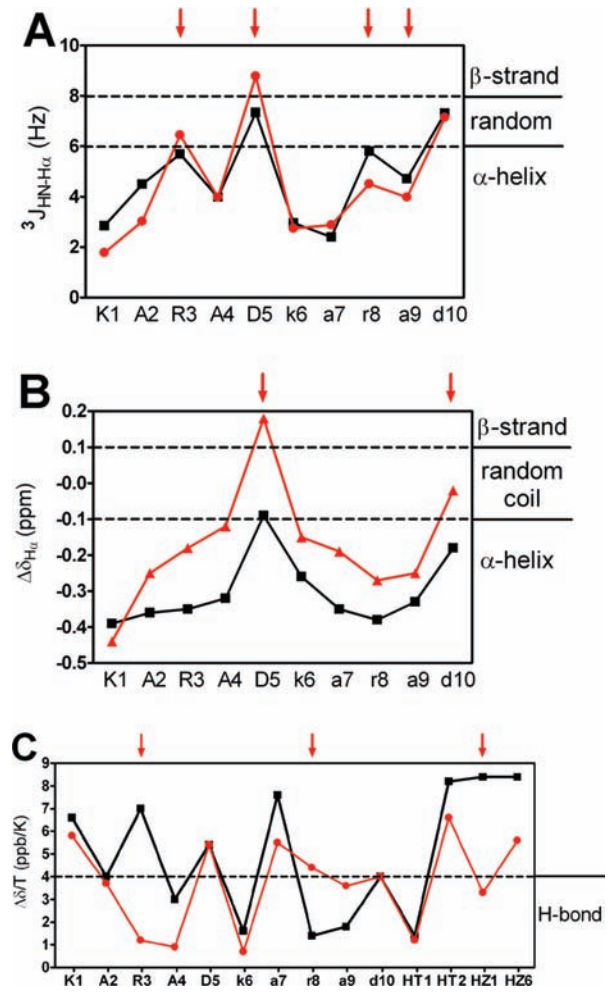

Figure 5. Comparison of ^{1}H NMR data for Ac−[KARAD][karad]−NH_2 (**7**) in 9:1 H_2O/D_2O (black), and 1:1 H_2O/d_3-TFE (red). (**A**): Variation in $^3J_{H\alpha\text{-}NH}$ coupling constants. (**B**): Differences between observed chemical shift and random coil values ($\Delta\delta = \delta - \delta_{random}$) for Hα. (**C**): Changes in the chemical shift of amide protons with temperature between 278−313 K. Red arrows indicate relevant changes in H_2O/d_3-TFE.

that hydrogen bonds would be lost, and Hα shifts and coupling constants would fall in the random coil region or at least at the edge of the helix region. Whereas this is somewhat true for the Hα shifts, it is not the case for temperature coefficients and coupling constants. It is also interesting to note that there are equivalent changes in the Hα shifts across the entire peptide and not just at the N-terminus, suggesting that perhaps the quantitative behavior of the Hα shifts in TFE/H_2O may not be interpreted in the same way as in plain aqueous buffer. Our conclusion that there is a major change in the N-terminal cycle and that the change manifests itself in residues Arg3 and Asp5 is based on several key pieces of evidence: First, by the observation of only the C-terminal macrocycle's signal in the CD spectrum. Second, for Arg3 there is an increase in $^3J_{H\alpha\text{-}NH}$ (>6 Hz) and the appearance of a hydrogen bond involving the Arg3 amide proton, which cannot be in an *i* to *i+4* fashion suggesting deviation from α-helicity. Third, for Asp5 a change toward an extended β-structure is evidenced by the change in both coupling constant and Hα chemical shift. Taken together, they provide compelling evidence that a change is occurring within the N-terminal macrocycle. To provide further confirmation, solution structures were calculated for NMR data acquired in H_2O/D_2O and H_2O/d_3-TFE.

Solution Structure for Ac−[KARAD][karad]−NH_2 (7) in Water. 2D NOESY spectra were acquired for **7** in H_2O/D_2O (9:1). A solution structure was calculated from a total of 78 NOE-derived distance restraints, 8 ϕ angle restraints, and 5 hydrogen-bond restraints. Hydrogen bond restraints were introduced in the final rounds of refinement and several combinations of potential carbonyl acceptors were used. Selection of final hydrogen-bond restraints was based on those that caused the fewest violations and had lower overall energies. There were no NOE violations >0.2 Å or dihedral angle violations >2°. Weak long-range $d_{\alpha N}(i\rightarrow i+3)$ and $d_{\alpha N}(i\rightarrow i+4)$ NOEs only occurred *within* respective cycles, there were no long-range NOEs between the two macrocycles. The best converged structures resulted from C═O→NH hydrogen bond restraints between the Acetyl→Arg4, Ala2→D-Lys6, Asp5→D-Arg8, Asp5→D-Ala9, D-Ala7→C-terminal amide. We rationalized the observation of low temperature coefficients and likely hydrogen bonding in the amide protons of both D-Arg8 and D-Ala9 as being due to the carbonyl oxygen of Asp5 forming a bifurcated ($i\rightarrow i+3$) and an ($i\rightarrow i+4$) hydrogen bond. Given the proximity of this carbonyl and the fact that the overall energies of this family of structures were lower compared to structures containing other possible H-bond patterns, this seems to be the most likely scenario. Overall, the structure gave a well-defined α_R-helical turn at the N-terminus followed by an α_L-helical turn at the C-terminus. This family of structures gave a good backbone superimposition over all residues (part A of Figure 6, rmsd 0.69), although the superimposition was much better when only the respective backbone atoms of the individual macrocycles were overlaid (parts B and C of Figure 6, rmsd residues 1−5: 0.22, residues 6−10: 0.32,). This suggested that, whereas a reasonably high proportion of helicity is maintained within each cycle, there is some flexibility between the two cycles.

Solution Structure for Ac−[KARAD][karad]−NH_2 (7) in Aqueous TFE. The solution structure was also determined for Ac−[KARAD][karad]−NH_2 (**7**) in H_2O/d_3-TFE (1:1) for comparison with the structure obtained in H_2O/D_2O. The solution structure was calculated from 106 NOE-derived distance restraints, 8 ϕ angle restraints, and 6 hydrogen-bond restraints. In H_2O/TFE (1:1), the structure was quite different with a clear bend at the junction between the two macrocycles (Figure 7). The bend brings the two macrocycles into close proximity to each other and this is corroborated by four long-range ($i\rightarrow i+5$) NOEs between Ala2 and D-Ala7 (part d of Figure 7) that were absent in the data acquired in H_2O/D_2O. The best converged structures had C═O→NH hydrogen bonds between the Acetyl→Arg3, Acetyl→Ala4, Lys1→Lys1HZ (lactam amide), Ala2→D-Lys6, Asp5→D-Ala9, D-Ala7→C-terminal amide proton(HT1) gave a tighter backbone superimposition than the H_2O/D_2O structure with an rmsd of 0.50 Å, once again better superimpositions of just the respective macrocycles were observed (Figure 7). The C-terminal D-cycle maintains an α_L-helical conformation, whereas the N-terminal L-cycle tightens with the acetyl cap forming two hydrogen bonds with the Arg3 and Ala4 amide protons, the Lys1 carbonyl forming a H-bond with its side chain amide proton. The large increase in the Asp5 dihedral angle facilitates the bend. The presence of a bend in the structure is interesting and has been observed in other polymer systems of mixed chirality in which helix reversal occurs.[12] Given that this appears to occur in the presence of TFE, it would seem that a hydrogen bond should form between a carbonyl in the all-L-residue macrocycle and an amide proton in the all-D-residue macrocycle, whereas in water the formation of this hydrogen bond is out-competed by water molecules. In peptidic structures where helix reversal or helix termination occurs (via the Schellman motif), $i\rightarrow i+5$ and $i+1\rightarrow i+4$

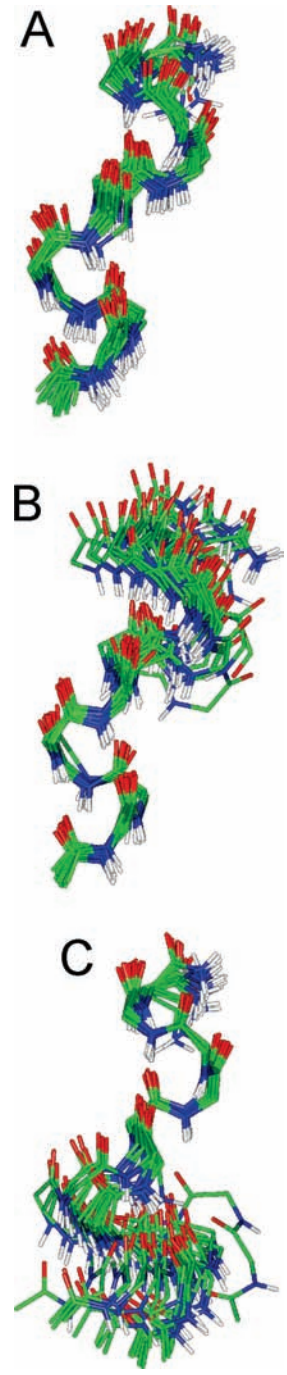

Figure 6. Final 20 lowest-energy NMR structures of Ac−[KARAD][karad]−NH_2 (**7**) in H_2O/D_2O (9:1). (**A**) Backbone superimposition of residues 1−10, (**B**) Backbone superimposition of residues 1−5, (**C**) Backbone superimposition of residues 6−10.

(12) Green, M. M.; Peterson, N. C.; Sato, T.; Teramoto, A.; Cook, R.; Lifson, S. *Science* **1995**, *268*, 1860–1866.

(13) (a) Datta, S.; Uma, M. V.; Shamala, N.; Balaram, P. *Biopolymers* **1999**, *50*, 13–22. (b) Datta, S.; Shamala, N.; Banerjee, A.; Pramanik, A.; Bhattacharjya, S.; Balaram, P. *J. Am. Chem. Soc.* **1997**, *119*, 9246–9251. (c) Aravinda, S.; Shamala, N.; Pramanik, A.; Das, C.; Balaram, P. *Biochem. Biophys. Res. Commun.* **2000**, *273*, 933–936.

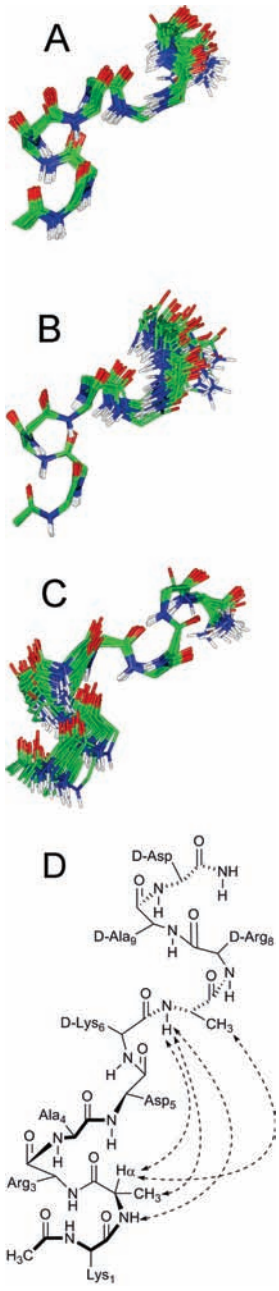

Figure 7. Final 20 lowest-energy NMR structures of Ac−[KARAD][karad]−NH_2 (**7**) in H_2O/d_3-TFE (1:1) with the N-terminus at the bottom. (**A**) Backbone superimposition of residues 1−10, (**B**) backbone superimposition of residues 1−5, (**C**) backbone superimposition of residues 6−10. (**D**) Four weak $i \rightarrow i + 5$ NOEs observed between Ala2 and D-Ala7 in H_2O/d_3-TFE, which corroborate the bend in the structure for **7**. These NOEs are not observed in the 2D NOESY spectrum in 90% H_2O/10% D_2O.

hydrogen bonds are commonly observed.[13] On examination of the NMR structures, the most likely participants in the $i \rightarrow i + 5$ hydrogen bond are the carbonyl oxygen of Ala2 and the amide proton of D-Ala7.

The Asp5 side chain carboxyl oxygen is not a H-bond partner. For the H_2O/D_2O structure, prospective partners for this carbonyl oxygen are either too distant or not at appropriate angles to form H-bonds. In H_2O/TFE, all calculated structures that included this hydrogen bond gave very high energies. This is in part because the Lys1 side chain amide proton is involved in a H-bond (i.e., pointing inward toward the helix), the trans-amide bond must place that carboxyl outward (away from the helix and possible amide protons to interact with). Therefore, the structure must unrealistically contort to accommodate a hydrogen bond with the Asp5 side chain carboxyl oxygen.

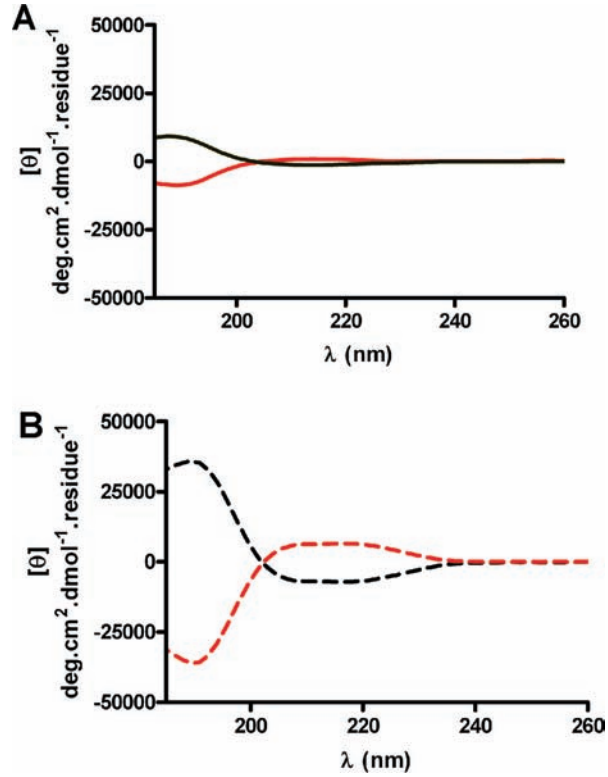

Figure 8. CD spectra for Ac−[KARAD]G[karad]−NH_2 (**9**, red; 100 μM) and Ac−[karad]G[KARAD]−NH_2 (**10**, black; 100 μM) at at 298 K in (**A**) 10 mM phosphate buffer (pH 7.2) and (**B**) 1:1 mixture TFE/phosphate buffer.

Interestingly, even though the NMR structures suggest that the formation of a hydrogen bond is possible, the variable-temperature NMR data suggests that the amide proton of D-Ala7 is not hydrogen bonded in water/TFE ($\Delta\delta/T$ = 5.5 ppb/K), however this temperature coefficient was significantly less than that observed in water (7.6 ppb/K), suggesting that it may be more shielded from the solvent. An $i + 1 \rightarrow i + 4$ hydrogen bond would also be expected to form between the Arg3-carbonyl oxygen and the D-Lys6 amide proton. Even though the temperature coefficient data suggests that the D-Lys6 amide proton is hydrogen bonded, analysis of the NMR structure reveals that the Arg3 carbonyl oxygen is oriented away from the D-macrocycle, ruling out the possibility of this type of hydrogen bond. Therefore, it seems that helix termination occurs through a distorted Schellman-like motif that is perhaps a consequence of the conformational restriction imposed by macrocyclization.

Effect of a Glycine Linker. We decided to separate the back-to-back macrocycles to investigate whether interactions between the two macrocycles led to this apparent conformational change. Compounds Ac−[KARAD]G[karad]−NH_2 (**9**) and Ac−[karad]G[KARAD]−NH_2 (**10**) were prepared with an achiral glycine spacer separating the macrocycles in an attempt to prevent the conformational change in TFE/buffer. Contrary to expectation, the observed CD spectra in both buffer and 1:1 TFE behaved in the same way (Figure 8).

Compound **9**, Ac−[KARAD]G[karad]−NH_2, was also investigated by NMR spectroscopy in both solvent systems (Figure

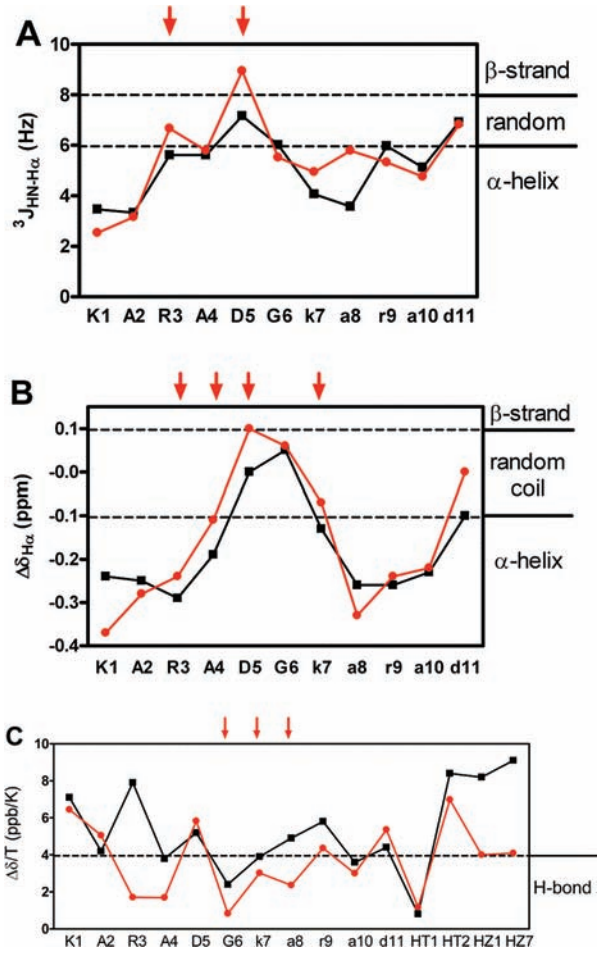

Figure 9. Summary of NMR data for Ac−[KARAD]G[karad]−NH_2 (**9**) in 9:1 H_2O/D_2O (black), and 1:1 H_2O/d_3-TFE (red). **A**. Variation in $^3J_{H\alpha\text{-}NH}$ coupling constants. **B**. Differences between observed chemical shift and random coil values ($\Delta\delta = \delta - \delta_{random}$) for Hα. **C**. Changes in the chemical shift of amide protons with temperature between 278−313 K. Red arrows indicate relevant changes in H_2O/d_3-TFE.

9) and the same trends were observed as for **7**. The coupling constants of Arg3 and Asp5 increase to a random coil and β-strand values respectively, there is a downfield shift in the Asp5 Hα resonance to a β-strand value (>0.1 ppm), and low-temperature coefficients were identical to those observed in **7** except around the hinge region (Gly6, D-Lys7, D-Ala8, Figure 10). The low-temperature coefficients indicate the formation of a Schellman-like motif in this hinge region due to increased flexibility by the addition of the glycine spacer. The temperature coefficients for **9** indicate that the D-Lys7 amide proton is involved in a hydrogen bond ($\Delta\delta/T = 3.1$ ppb/K), which could only be achieved with the Ala2 carbonyl oxygen and would constitute an $i \rightarrow -i + 5$ hydrogen bond. Given the similarity in the NMR data and CD spectra, it is likely that the N-terminal cycle undergoes Schellman-like helix termination, whereas the C-terminal cycle is preserved. It is intriguing that the formation of new hydrogen bonds in the hinge region is not an absolute requirement for the structural change as it is not observed for **7** but is observed for **9**. A similar type of helix reversal mediated by a Schellman motif has previously been proposed in synthetic peptides with 4−24 L-leucine residues attached to an achiral

(14) Ousaki, N.; Inai, Y. *J. Am. Chem. Soc.* **2006**, *128*, 14736–14737.

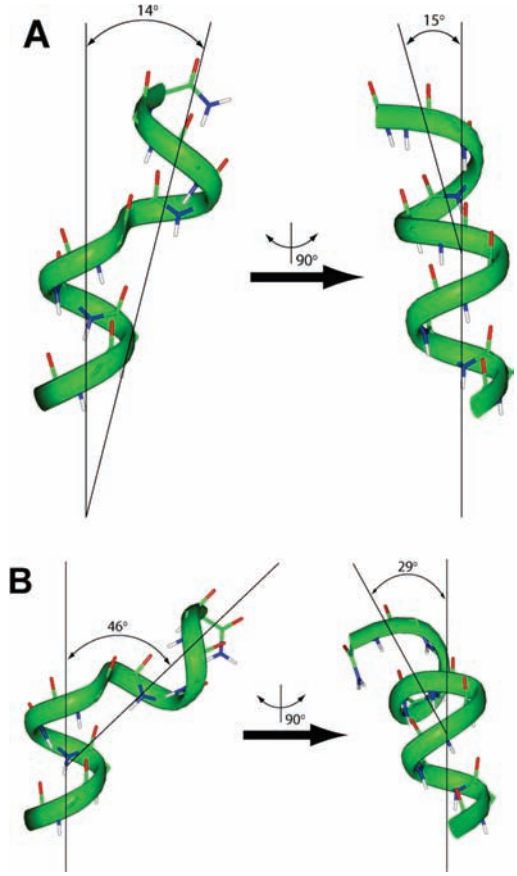

Figure 10. Conformational switch: changes in angle of the C-terminal cycle relative to the N-terminal cycle for the average structure of the 20 lowest-energy conformations of **7** in 9:1 H_2O/D_2O (**A**), and 1:1 H_2O/TFE (**B**), with N-terminus at the bottom. Structure on the left-hand side in both cases represents the *sagittal* plane, whereas the structures on the right-hand side represent the *coronal* plane.

region of four Aib-dehydrophenylalanine repeats, although the structure of these molecules did not show any solvent dependence.[14]

Summary of Conformational Changes Induced by TFE. The change from continuous to bent conformations in **7** is dramatically represented by the change in angle of the C-terminal cycle relative to the N-terminal cycle (Figure 10). In the average structure of 20 lowest-energy conformations **7** in H_2O/D_2O (9:1), the axis of the C-terminal cycle is normally slightly offset from the axis of N-terminal cycle by 14° and 15° along the two longitudinal planes. Given that the family of NMR structures in H_2O/D_2O suggests some flexibility between the two cycles, it is likely that this angle could alter to 0°, with both helical axes being parallel to one another. In the presence of 50% TFE, the average structure suggests a 32° shift (14 ± 4°→46 ± 2°) along the sagital plane and a smaller 14° change along the coronal plane (15 ± 3°→29 ± 2°).

For **7** and **8**, the dramatic difference in the CD curves in the two solvents is not due to aggregation. There was no concentration dependence of CD spectra for **6** in 10 mM PBS (pH 7.4, 298 K) in the range 18−720 μM (Figure S14 of the Supporting Information) or for **8** in the range 30−1500 μM (Figure S16 of the Supporting Information). By monitoring the molar ellipticity at 215 nm, we have shown that increasing % TFE in such solutions of **8** leads to 50% conversion to the bent structure with 20% TFE added, whereas complete conversion requires about 50% TFE (Figure S15 of the Supporting Information).

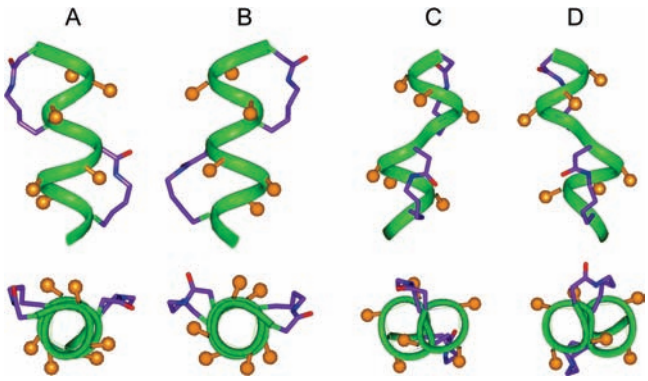

Figure 11. Homo- and heterochiral scaffolds from combinations of homochiral cyclic pentapeptide units [KARAD] and/or [karad]. (**A**) Ac−[KARAD][KARAD]−NH_2 (**5**); (**B**) Ac−[karad][karad]−NH_2, (**6**); (**C**) Ac−[KARAD][karad]−NH_2, (**7**); (**D**) Ac−[karad][KARAD]−NH_2 (**8**). Backbone - green ribbon, lactam bridges - purple, side chains available for substitution - orange; N-terminus at bottom.

Moreover, the CD spectrum for **8** in 8 M guanidine was indistinguishable from the spectrum in 10 mM PBS (pH 7.4), indicating its conformational stability and disaggregated nature.

Nanomaterials are currently being sought with properties that can be altered in responses to different external triggers, interconverting between structures with different function. Such smart materials are finding valuable applications in materials research,[15] for example in self-assembling systems capable of switching between fluids and hydrogels depending on their concentration,[16] or hydrogen bonding ability of their solvent environment.[17] Current approaches primarily examine properties of end products, rather than beginning with smaller units of defined structure with defined switches and then incorporating them into larger systems. The finding here of a structural hinge that responds to an external cue could be a useful pointer to a bottom up approach to smart materials.

Novel Scaffold Library. We have thus summarized a series of novel constrained alpha helices (α_L, α_R, $\alpha_R\alpha_R$, $\alpha_L\alpha_L$, $\alpha_L\alpha_R$, $\alpha_R\alpha_L$, α_LGlyα_R, α_RGlyα_R) based on the highly water-stable α-helical cyclic pentapeptide modules **1** and **2**. These interesting homochiral and heterchiral helical structures each present their amino acid side chains in unique 3D space, as shown for **5**−**8** in Figure 11. These novel scaffolds are limited by immutable amino acid side chains at certain positions within the helix but still tolerate diverse modifications[11] to 60% of their amino acids, and each structure has a unique spatial distribution of their amino acid side chains. It is likely that the tolerance of the scaffolds herein to changes in internal residues (positions 2, 3, 4, 7, 8, 9) will mirror that previously observed for the monocyclic pentapeptide,[11] that is, residues with moderate to high helix propensity (e.g., Ala, Leu, Met, Gln, Phe, etc.) within proteins will be tolerated, whereas those that do not favor helicity in proteins (e.g., Ser, Gly) will not. On the otherhand, the K and D residues at positions 1, 5, 6, 10 cannot be changed.[11] Given the enantiomeric nature of **7** and **8**, compound **8** would be expected to form a well-defined left-handed α-helical turn at the N-terminus followed by a right-handed α-helical turn at the C-terminus. In the case of **6**−**8** (parts B−D of Figure 11), the positions occupied by the side chains are not replicated by any standard natural systems of which we are aware. Given that short right-handed (L-residue) helices or left-handed (D-residue) helices are known to modulate protein−protein interactions, dual handed α-helices are a logical extension and add to the repertoire of peptidomimetic scaffolds for interacting with biological receptors.

Theoretical studies have suggested that structures such as these may prove useful in making productive interactions with biological receptors that would not otherwise be achievable using the standard protein mimicry techniques. A heterochiral helix composed of a α_L-helical segment followed by a α_R-helical segment (such as **8**) has been proposed[18] to be a potential scaffold for interaction with an α_L-helical target. Thus, a heterochiral scaffold composed of a right α_R-helical segment followed by a α_L-helical segment (such as **7**) might similarly be expected to be capable of interaction with an α_R-helical target. This system of heterochiral helices represented by **7** and **8** appears to offer promising opportunities to test hypotheses in relation to targeting proteins with defined helical motifs and modules.

Conclusions

We have generated novel and highly stable homochiral and heterochiral helices through the modular assembly of discrete elements of conformationally predefined right- and left-handed α-helical turns. These structures undergo inversion of helical sense at their centers resulting in two solvent-dependent conformations. In water, all of the structures examined here (α_L, α_R, $\alpha_L\alpha_L$, $\alpha_R\alpha_R$, $\alpha_L\alpha_R$, $\alpha_R\alpha_L$) exhibit continuous left- or right-handed alpha helices in which individual turns maintain their respective structural integrity. When 50% TFE is introduced into their aqueous solution, the homochiral structures (α_L, α_R, $\alpha_L\alpha_L$, $\alpha_R\alpha_R$) do not change but the heterochiral structures ($\alpha_L\alpha_R$, $\alpha_R\alpha_L$) display reduced helicity in the N-terminal cyclic component associated with large changes in the dihedral angles of residues R3 and D5 (regardless of whether a glycine spacer is present). This subtle solvent-dependent conformational switch is caused by heterochiral helical turns being able to approach one another through the bend accessible by their joining, enabling intercyclic intramolecular H-bonding. By contrast, the homochiral compounds are extended helices with a continuous hydrogen-bonding network, including helix-defining intramolecular hydrogen bonds between the two macrocycles. Homochiral helices have perfect alignment of hydrogen-bond donors and acceptors throughout their bicyclic components, thus no solvent-induced conformational change can occur. However, the bent heterochiral structure repositions the C-terminal helix by nearly 30° and 45° along its two longitudinal planes. This large structural change in response to an external cue, a change to the polarity of the solvent in this case with the less-polar TFE encouraging intramolecular hydrogen bonding, suggests the possible use of this molecular unit as a conformational switch or hinge within larger structures to generate smart materials. In addition, this library of left- and right-handed **1**−**3** turn helical compounds comprises a potentially valuable group of new scaffolds that project amino acid side chains into unique 3D space and these could also be valuable new materials for probing

(15) Fairman, R.; Akerfeldt, S. S. *Curr. Opin. Struct. Biol.* **2005**, *15*, 453–463.
(16) (a) Fishwick, C. W. G.; Beevers, A. J.; Carrick, L. M.; Whitehouse, C. D.; Aggeli, A.; Boden, N. *Nano Lett.* **2003**, *3*, 1475–1479. (b) Whitehouse, C.; Fang, J. Y.; Aggeli, A.; Bell, M.; Brydson, R.; Fishwick, C. W. G.; Henderson, J. R.; Knobler, C. M.; Owens, R. W.; Thomson, N. H. *Angew. Chem., Int. Ed. Engl.* **2005**, *44*, 1965–1968.
(17) (a) Ryadnov, M. G.; Woolfson, D. N. *Angew. Chem., Int. Ed. Engl.* **2003**, *42*, 3021–3023. (b) Altman, M.; Lee, P.; Rich, A.; Zhang, S. *Protein Sci.* **2000**, *9*, 1095–1105.
(18) Nanda, V.; DeGrado, W. F. *J. Am. Chem. Soc.* **2006**, *128*, 809–816.

interactions with macromolecules in chemistry, materials, and biological research.

Experimental Section

General Reagents. Fmoc−Asp(OPip)−OH and Fmoc-D-Asp(OPip)−OH were obtained from Bachem (Bubendorf, Switzerland). Fmoc-Lys(Mtt)−OH, Fmoc-D-Lys(Mtt)−OH, and other L-amino acids, Rink amide MBHA LL, and Rink Amide MBHA resins were obtained from Novabiochem (Melbourne, Australia). Benzotriazol-1-yl-1,1,3,3-tetramethyluronium (HBTU) and benzotriazol-1-yloxy-tris(dimethylamino)-phosphonium (BOP) were obtained from Iris Biotech (Germany). Dimethylformamide, diisopropylethylamine, trifluoroacetic acid, and other reagents were of peptide synthesis grade and obtained from Auspep (Melbourne, Australia). Triisopropylsilane and dichloromethane were obtained from Sigma-Aldrich (Sydney, Australia).

Synthesis of Helices of Cycles 1−10. Monocyclic and bicyclic peptides were prepared using a method previously described[11] on a 0.16 mmol scale by manual stepwise Fmoc solid-phase peptide synthesis. The phenylisopropyl ester of an aspartic acid and methyltrityl group of lysine were removed by treating the peptide resin with 3% TFA in DCM (5 × 2 min). The resin was neutralized by washing with 5% DIPEA in DMF (2 × 3 min). Cyclization was effected on-resin using BOP, HOAt, DIPEA in DMSO/NMP (1:1). The same procedure was repeated to generate a second cycle as required. The peptide resin was then washed with DMF, MeOH/DCM, and DCM, dried under nitrogen with suction for 2 h. Peptides were cleaved using 95% TFA, 2.5% TIPS, 2.5% H_2O. Peptides were precipitated with cold diethyl ether and then decanted to give white solids that were redissolved in 1:1 acetonitrile/water and lyophilized. The crude peptides were purified by rp-HPLC (R_{t1}: Vydac C18 column, 300 Å. Twenty-two × 250 mm, 214 nm, Solvent A = 0.1% TFA in H_2O, Solvent B = 0.1% TFA, 10% H_2O in acetonitrile. Gradient: 0% B to 70% B over 35 min). *Ac−(cyclo-1,5)−[KARAD]−NH*$_2$ (**1**): 62 mg (43% isolated). R_{t1}: 13.8 min. HRMS $[M + H]^+$ = 583.33 (found), 583.33 (Calcd). *Ac−(cyclo-1,5)−[karad]−NH*$_2$ (**2**): 44 mg (23% isolated). R_{t1}: 13.8 min. HRMS $[M + H]^+$ = 583.13 (found), 583.33 (Calcd). *Ac−(cyclo-2,6)−R[KAAAD]-−H*$_2$ (**3**): 75 mg (46% isolated). R_{t1}: 13.7 min. HRMS $[M + H]^+$ = 655.37 (found), 655.37 (Calcd). *Ac−(cyclo-2,6)−r[kaaad]−NH*$_2$ (**4**): 60 mg (27% isolated). R_{t1}: 13.7 min. HRMS $[M + H]^+$ = 655.28 (found), 655.37 (Calcd). *Ac−(cyclo1-5,6-10-[KARAD][KARAD]−NH*$_2$ (**5**): 19 mg (10% isolated). ESMS: [obs. $(M + 2H^+)/2$ 554.04] [Calcd $(M + 2H^+)/2$ 554.30]. R_{t1}: 14.8 min. *Ac−(cyclo1−5,6−10−[karad][karad]−NH*$_2$ (**6**): 25 mg (15% isolated). ESMS: [obs. $(M + 2H^+)/2$ 554.23] [Calcd $(M+2H^+)/2$ 554.30]. R_{t1}: 14.8 min. *Ac−(cyclo1-5,6-10-[KARAD][karad]−NH*$_2$ (**7**): 22 mg (6.6% isolated). ESMS: [obs. $(M + 2H^+)/2$ 553.62] [Calcd $(M+2H^+)/2$ 553.30]. R_{t1}: 14.5 min. *Ac−(cyclo1-5,6-10-[karad][KARAD]−NH*$_2$ (**8**): 3 mg (1% isolated). ESMS: [obs. $(M + 2H^+)/2$ 553.62] [Calcd $(M + 2H^+)/2$ 553.30]. R_{t1}: 14.5 min. *Ac−(cyclo1-5,6-10-[KARAD]G[karad]−NH*$_2$ (**9**): 9 mg (2.6% isolated). ESMS: [obs. $(M + 2H^+)/2$ 582.15] [Calcd $(M + 2H^+)/2$ 581.65]. R_{t1}: 14.7 min. *Ac−(cyclo1-5,6-10-[karad]G[KARAD]−NH*$_2$ (**10**) 2 mg (0.6% isolated). ESMS: [obs. $(M + 2H^+)/2$ 582.14] [Calcd $(M + 2H^+)/2$ 581.65]. R_{t1}: 14.7 min. More characterization data is provided in the Supporting Information.

NMR Spectroscopy. Samples for NMR analysis were prepared by dissolving peptides (2 mg) in 550 μL H_2O and 50 μL D_2O (5 mmol) and adjusting the pH of the solution to ∼3.5 by adding HCl or NaOH and stirring for 30 min. 1D and 2D ^{1}H NMR spectra were recorded on Bruker Avance DRX-600 spectrometers at 288K. All spectra were recorded in the phase-sensitive mode using time-proportional phasing incrementation.[19] 2D experiments included TOCSY using MLEV-17 spin lock sequence with a mixing time of 80−100 ms, ROESY with a mixing time of 250 ms, and NOESY with a mixing time of 300 ms. Water suppression was achieved using watergate W5 pulse sequences with gradients using double echo.[20] 2D TOCSY, ROESY, and NOESY experiments were recorded over 6620.5 Hz with 4 096 complex data points in F2 and 512−1024 increments in F1 with 16 and 48 scans per increment, respectively. Spectra were processed using XWINNMR (Bruker, Germany). The $t1$ dimensions of all 2D spectra were zero filled with 2048 real data points, and 90° phase-shifted sine bell window functions applied in both dimensions followed by Fourier transformation, and fifth-order polynomial baseline correction. Chemical shifts were referenced to DSS an internal standard at 0.00 ppm. Processed spectra were analyzed using the program *SparkyNMR*[21] and assigned using the sequential assignment technique.[22]

Structure Calculations. Cross peaks in NOESY spectra were integrated and calibrated in *SparkyNMR*,[21] distance constraints derived using the standard CALIBA function in *DYANA*.[23] Corrections for pseudo-atoms were added to distance constraints where needed. Backbone dihedral angle restraints were inferred from $^3J_{NHCHa}$ coupling constants in 1D spectra at 288 K, ϕ was restrained to $-65 \pm 30°$ for $^3J_{NHCHa} \leq 6$ Hz, or $-120 \pm 30°$ for $^3J_{NHCHa} \geq 8$ Hz. Peptide bond ω angles were all set to trans, and structures were calculation without explicit hydrogen-bond restraints. Initial structures were generated using ANNEAL function in *DYANA*. Several rounds of refinement in *DYANA* yielded optimized NOE-derived distance restraints, ϕ angle restraints, and hydrogen-bond restraints, which were then used for structure calculations in *XPLOR 3.851*.[24] Starting structures with randomized ϕ and ψ angles and extended side chains were generated using an ab initio simulated annealing protocol.[25] The calculations were performed using the standard forcefield parameter set (PARALLHDG.PRO) and topology file (TOPALLHDG.PRO) in *XPLOR* with in-house modifications to generated lactam bridges between lysine and aspartic acid residues. Refinement of structures was achieved using the conjugate gradient Powell alogrithm with 1000 cycles of energy minimization and a refined forcefield based on the program *CHARMm*[26] Structures were visualized with *MOLMOL*[27] and *InsightII*.[28]

Circular Dichroism Spectroscopy. CD experiments were performed on a Jasco Model J-710 spectropolarimeter that was routinely calibrated with (1S)-(+)-10-camphorsulfonic acid. Spectra were recorded in a 0.1 cm Jasco cell between 260 and 185 at 50 nm/min with a bandwidth of 1.0 nm, response time of 2 s, resolution step width of 0.1 nm, and sensitivity of 20, 50, or 100 mdeg. Each spectrum represents the average of 5 scans with smoothing to reduce noise. Peptide samples for CD spectroscopy were dissolved in 1 mL of 18 MΩ distilled water (∼5−10 mg/mL). 500 μL of each stock solution was then diluted 1:1 with phosphate buffer pH 7.4, whereas the remaining 500 μL was kept for concentration determination. Solutions were then prepared for each sample with final concentrations ranging from 50 − 800 mM in 10 mM sodium phosphate buffer (pH7.4), with or without 2,2,2-trifluoroethanol (TFE). Over this concentration range, the CD intensity was found to be independent of concentration ruling out aggregation as a stabilizing effect. The remaining 500 μL from the initial stock solution was used for accurate concentration determination.

(19) Marion, D.; Wuthrich, K. *Biochem. Biophys. Res. Commun.* **1983**, *113*, 967–974.
(20) Liu, M. L.; Mao, X. A.; Ye, C. H.; Huang, H.; Nicholson, J. K.; Lindon, J. C. *J. Magn. Reson.* **1998**, *132*, 125–129.
(21) Goddard, T. D.; Kneller, D. G. *SPARKY 3*; University of California: San Francisco.
(22) Wuthrich, K. *NMR of Proteins and Nucleic Acids*; Wiley-Interscience: New York, 1986.
(23) Guntert, P.; Mumenthaler, C.; Wuthrich, K. *J. Mol. Biol.* **1997**, *273*, 283–298.
(24) Brunger, A. T. *Xplor 3.81*; Yale University: New Haven, CT, 1992.
(25) Nilges, M.; Gronenborn, A. M.; Brunger, A. T.; Clore, G. M. *Protein Eng.* **1988**, *2*, 27–38.
(26) Brooks, B. R.; Bruccoleri, R. E.; Olafson, B. D.; States, D. J.; Swaminathan, S.; Karplus, M. *J. Comput. Chem.* **1983**, *4*, 187–217.
(27) Koradi, R.; Billeter, M.; Wuthrich, K. *J. Mol. Graphics* **1996**, *14*, 51.
(28) *InsightII*, Version2000 ed.; Molecular Simulations Inc.: San Diego, CA.

Concentrations of these solutions were then determined using the PULCON method.[29] 90° pulses were accurately determined and then 1D spectra were acquired using the standard Watergate sequence with a ns = 64, rg 128, d1 = 25s. Fully resolved and most downfield amide resonances were integrated and used to calculate the concentration from the equation:

$$c_u = c_R \frac{S_U T_U \vartheta_{360}^U n_R r g_R}{S_R T_R \vartheta_{360}^R n_U r g_U}$$

where c is the concentration, S is the integral(in absolute units)/number of protons, T is the temperature in Kelvin, q_{360} is the 360° rf pulse, n is the number of scans, and rg is the receiver gain used for measuring the reference (R) and unknown (U) samples. Temperature-dependent experiments were conducted between 5−85 °C in 5 °C increments and were temperature controlled using a Neslab RTE-111 circulating water bath and a PTC-423 thermostatted cell holder. Once the desired temperature was reached, a 10 min equilibration time was allowed before full wavelength scan CD spectra were recorded as described above. CD data in ellipticity was converted to mean peptide ellipticity: $[q] = q/(10 \times C \times N_p \times l)$, where q is the ellipticity in millidegrees, C is the peptide molar concentration (M), l is the cell path length (cm), and N_p is the number of peptide units.

Acknowledgment. The Australian Research Council (ARC) and the National Health and Medical Research Council of Australia (NHMRC) provided financial support for this research, while the ARC provided a Federation Fellowship to D.F.

Supporting Information Available: Tables and figures of CD spectral data, 1D and 2D ^{1}H NMR spectra, NOE tables, temperature coefficients, as well as data for the determination or interpretation of 3D structures for **1**−**10** (28 pages). This material is available free of charge via the Internet at http://pubs.acs.org.

JA9065283

(29) Wider, G.; Dreier, L. *J. Am. Soc. Chem.* **2006**, *128*, 2571–2576.